Regular paper

Field: Biochemistry General

Topic: Protein Interaction and Recognition

Dynamic Assembly Properties of Nonmuscle Myosin II Isoforms Revealed by Combination of Fluorescence Correlation Spectroscopy and Fluorescence Cross-Correlation Spectroscopy

Mariko Mitsuhashi[1]†, Hiroshi Sakata[2]†, Masataka Kinjo[2], Michio Yazawa[1], and Masayuki Takahashi[1]*

[1] *Division of Chemistry, Faculty of Science, Hokkaido University, Sapporo 060-0810;*

[2] *Laboratory of Molecular Cell Dynamics, Faculty of Advanced Life Science, Hokkaido University Sapporo 001-0021, Japan*

Running title: FCCS analysis of myosin II assembly

†These authors contributed equally to this work.

*Corresponding author: Masayuki Takahashi, Division of Chemistry, Graduate School of Science, Hokkaido University, Sapporo 060-0810, Japan. Tel: 81-11-706-3814, Fax: 81-11-706-4924. E-mail: takahash@sci.hokudai.ac.jp

Abbreviations: BRF, MHC-IIB rod fragment; ARF, MHC-IIA rod fragment; FCS, fluorescence correlation spectroscopy; FCCS, fluorescence cross-correlation spectroscopy, TCEP, tris(2-carboxyethyl)phosphine hydrochloride.

Summary

Myosin II molecules assemble into filaments through their C-terminal rod region, and are responsible for several cellular motile activities. Three isoforms of nonmuscle myosin II (IIA, IIB and IIC) are expressed in mammalian cells. However, little is known regarding the isoform composition in filaments. To obtain new insight into the assembly properties of myosin II isoforms, especially regarding the isoform composition in filaments, we performed a combination analysis of fluorescence correlation spectroscopy (FCS) and fluorescence cross-correlation spectroscopy (FCCS), which enables us to acquire information on both the interaction and the size of each molecule simultaneously. Using C-terminal rod fragments of IIA and IIB (ARF296 and BRF305) labeled with different fluorescent probes, we demonstrated that hetero-assemblies were formed from a mixture of ARF296 and BRF305, and that dynamic exchange of rod fragments occurred between pre-formed homo-assemblies of each isoform in an isoform-independent manner. We also showed that Mts1 (S100A4) specifically stripped ARF296 away from the hetero-assemblies, and consequently, homo-assemblies of BRF305 were formed. These results suggest that IIA and IIB can form hetero-filaments in an isoform-independent manner, and that a factor like Mts1 can remove one isoform from the hetero-filament, resulting in a formation of homo-filaments consisting of another isoform.

Key words: myosin II, assembly, FCS, FCCS, Mts1 (S100A4)

Introduction

Myosins constitute a superfamily of actin-based motor proteins (*1*). All members of the myosin family have a highly conserved globular motor domain that contains an actin-binding region and an ATPase region, followed by a neck domain to which the light-chains bind, and a variety of functionally specialized C-terminal tail regions (*1, 2*). Myosin II, one of the best-studied members of the superfamily, is composed of two heavy chains (MHCs) and two pairs of light chains. The tail of myosin II forms an α-helical coiled-coil rod-like structure, and is involved in the assembly of myosin II molecules into filaments (*1-3*). It has been shown that the C-terminal region of the rod is involved in filament formation of myosin II molecules (*4-7*). To perform its contractile functions with actin filaments, myosin II must be assembled into filaments.

All vertebrate cells, including muscle cells, contain a form of myosin II referred to as nonmuscle myosin II, which functions in a number of cellular processes such as cytokinesis, migration, morphogenesis and adhesion (*1, 8, 9*). The dynamic filament assembly-disassembly transitions of myosin II molecules are particularly important in nonmuscle cells. In mammalian cells, there are three different isoforms of nonmuscle MHCs referred to as MHC-IIA, MHC-IIB and MHC-IIC (*10-13*), which together with two pairs of light chains form nonmuscle myosin IIA, myosin IIB and myosin IIC, respectively. These three isoforms are expressed in a tissue-dependent manner (*13*), and display distinct properties with respect to ATPase and motor activities (*13-15*). Concerning two of the isoforms, IIA and IIB, the functional differences are suggested by the phenotypes following their ablation in mice (*16-18*), or by their distinct subcellular localization (*19-21*). To function effectively, it is reasonable to consider that they assemble in an isoform-specific mode to form homo-filaments (homogeneous with respect to their subunit composition) in cells. However, little has been reported regarding the isoform composition in filaments except for a few *in vitro* studies. Murakami *et al*. demonstrated that the rod fragments of myosin IIA and IIB would coassemble *in vitro* as judged by their salt-dependent solubility (*22*).

The *mts1* gene has been isolated as a gene expressed at high level in metastatic cells, and also been observed in normal tissues (*23*). The protein product of the *mts1* gene, Mts1 (also known as S100A4), a member of S100 family of Ca^{2+}-binding proteins, is generally homodimer and interacts with a number of protein targets in a Ca^{2+}-dependent manner (*24*). Nonmuscle myosin IIA was identified as one of the target proteins of Mts1 (*25, 26*) and its C-terminal region was found to function as the binding site (*27, 28*). Interestingly, Mts1 binding keeps the myosin IIA rod fragments in a disassembled state, whereas Mts1 has little effect on the assembly properties of myosin IIB (*22, 28*).

Fluorescence correlation spectroscopy (FCS) is an extremely sensitive method based on the fluctuation analysis of fluorescence intensity coming from a small and fixed confocal volume element to detect and characterize fluorescent molecules in a homogeneous solution (*29-31*). FCS provides the average number of fluorescent molecules in a confocal volume and the diffusion time of the molecules passing through the confocal area by Brownian motion. A diffusion coefficient evaluated from the diffusion time reflects a size of the fluorescent molecules and its molecular complex. These properties would be useful for the analysis of the dynamic process of filament formation of myosin II molecules. Dual color fluorescence cross-correlation spectroscopy (FCCS), an extended approach of the standard FCS, can detect the coincidence between two molecules labeled with spectrally distinct fluorescent probes in an overlapping confocal volume (*31, 32*). FCCS has been used to analyze the association-dissociation reaction and interaction of two molecular species. This property would be helpful for the determination of myosin II isoform composition in filaments.

If myosin II isoforms assemble into homo-filaments, it seems likely that some self-recognition mechanisms of individual myosin II isoforms exist. We have found that exogenous expression of the rod fragments consisting of 305 amino acid residues from the C-terminal end of myosin IIB (BRF305) in the cultured cells induced an unstable cell shape similar to MHC-$IIB^{-/-}$ fibroblasts (*33*). The myosin IIA rod fragments ARF296 corresponding to BRF305 did not exhibit this effect. BRF305 includes the critical regions for the assembly (7) as

well as the nonhelical tailpiece, which is the most distinct portion in primary structure among isoforms. This dominant negative effect was caused by an isoform-specific manner, raising the possibility that BRF305 can distinguish myosin IIB from myosin IIA in the living cell.

To obtain new insights into the assembly properties, especially in regards to the isoform composition of nonmuscle myosin II filaments, we carried out the single-molecule level analyses of FCS and FCCS experiments using the rod fragments, BRF305 and ARF296, labeled with fluorescent probes. The results indicated that BRF305 and ARF296 coassembled irrespective of specific isoform recognition, and that dynamic exchange of subunits occurred between pre-formed homo-assemblies of each isoform. Moreover, the results indicated that Mts1 specifically stripped ARF296 away from the pre-formed hetero-assemblies, and consequently, homo-assemblies of BRF305 were formed.

Materials and Methods

Plasmid Construction

The cDNAs encoding the MHC-IIA rod fragment (ARF296, Leu 1666-Glu 1961; 32 kDa) and the MHC-IIB rod fragment (BRF305, Phe 1672-Glu 1976; 33 kDa) were amplified from a human brain cDNA library (Clontech, Mountain View, CA, USA) as a template, and primer sets of 5'-CGCGGATCCGCTGGCCCAGGCCAAAGAGAACCAG-3' (forward) and 5'-CGCGGATCCTTATTCGGCAGGTTTGGCCTC-3' (reverse), and 5'-CGCGGATCCGTTTGCTCAATCCAAAGAGAGTGAA-3' (forward) and 5'-CGCGGATCCTTACTCTGACTGGGGTGGCTG-3' (reverse), respectively. *Bam* HI sites are indicated by underline. The amplified DNA was digested with *Bam* HI and subcloned into a *Bam* HI site of the pET-15b vector (Novagen, Madison, WI, USA). Furthermore, addition of a single Cys residue at the N-terminus of ARF296 and BRF305 and conversion of Cys 1835 in ARF296 to Ser were achieved by the PCR method of Weiner *et al.* (*34*). The MHC-IIA sequences of rat, chicken and *Xenopus* have a Ser residue at this position.

The cDNA encoding Mts1 was amplified by PCR using the human brain cDNA library (Clontech) as a template, and primer set of 5'-CATATGGCGTGCCCTCTGGAGAAGGCC-3' (forward) and 5'-GGATCCTCATTTCTTCCTGGGCTGCTTATG-3' (reverse). *Nde* I and *Bam* HI sites are underlined, respectively. The amplified DNA was digested with *Nde* I and *Bam* HI, and subcloned into the *Nde* I and *Bam* HI site of pET15b vector to obtain plasmid pET-Mts1. The entire nucleotide sequence of the amplified DNA was confirmed by sequencing using a sequencer (ABI PRISM 310; Applied Biosystems, Foster City, CA, USA).

Expression and Purification of Recombinant Proteins

Expression and purification of the recombinant rod fragments were performed as described previously (*7*) with the following modifications. To prevent undesirable degradation, 5 μg/ml pepstatin A, 5 μg/ml aprotinin, 5 μg/ml leupeptin, 50 μg/ml TLCK and 100 μg/ml TPCK were added to the binding buffer besides 0.1 mM PMSF. The purified recombinant proteins were

digested with 2.5 units of thrombin/mg of protein in high salt buffer (20 mM sodium phosphate (pH7.2), 500 mM NaCl) for 16 h at 4 °C, and the digested proteins were loaded onto a Ni^{2+} affinity resin column (His-Bind; Novagen) again to remove any undigested proteins and the short His-tag leader completely. The flow-through fraction was dialyzed against a buffer containing 20 mM sodium phosphate (pH 7.2) and 500 mM NaCl, and the concentration of the purified proteins was adjusted to 1 mg/ml. Each of the resulting rod fragments contains an extra sequence of Gly-Ser-His-Met-Leu-Glu-Asp-Pro-Cys at the N-terminus.

Recombinant Mts1 protein was expressed in *Escherichia coli* BL21(DE3)pLysS, transformed with pET-Mts1. Expression and purification of the recombinant proteins were performed as described previously (*7*) with the following modifications. The cells were cultured in 500 ml of LB medium. To prevent undesirable degradation, 5 μg/ml pepstatin A, 5 μg/ml aprotinin, 5 μg/ml leupeptin, were added to the binding buffer besides 0.1 mM PMSF. The purified recombinant Mts1 was digested with 2.5 units of thrombin/mg of protein in low salt buffer (20 mM Tris-HCl (pH7.5), 50 mM NaCl) for 16 h at 4 °C, and the concentration of the purified proteins was adjusted to 1.2 mg/ml. Purified recombinant Mts1 was stored at –80°C.

The protein concentrations were determined by the biuret method or by Bio-Rad Protein Assay (Bio-Rad, Hercules, CA, USA) using BSA as a standard.

Labeling of Fragments with Fluorophores

Rod fragments, ARF296 and BRF305, were labeled with either Alexa Fluor 633 C_5 maleimide or Alexa Fluor 488 C_5 maleimide (Molecular Probes, Eugene, OR, USA) through the N-terminal extra Cys residue according to a manufacture's protocol with the following modifications. In brief, the fragments were incubated with 90 μg/ml TCEP in 50 mM Tris-HCl (pH 7.5) for 10 min at 25°C to reduce the disulfide bond of Cys residues. The fluorophores dissolved in DMSO were added in 10~20-fold molar excess over the proteins, and the reaction was allowed to proceed overnight at 4°C. The free dyes were removed by dialysis against a solution containing 20 mM sodium phosphate (pH 6.0), 50 mM NaCl and 2 mM $MgCl_2$. The assembled ARF and BRF

fragments formed during dialysis were collected by centrifugation at 420000 g and 21000 g for 20 min at 4°C, respectively. The pellet was dissolved in a high salt buffer (20 mM sodium phosphate (pH7.2), 500 mM NaCl), and the solution was passed through a Sephadex G-25 Medium (GE Healthcare Bio-Sciences, Piscataway, NJ, USA) column equilibrated with the high salt buffer to remove residual amount of free dyes. The samples were finally ultracentrifuged at 420000 g for 20 min at 4°C to remove residual amount of insoluble materials.

FCS and FCCS measurements

FCS and FCCS measurements were carried out using an LSM 510 + ConfoCor2 instrument (Carl Zeiss, Oberkochen, Germany) with a 40 × 1.2 water objective, which allows simultaneous excitation at 488 nm and 633 nm by Argon-ion and Helium-Neon Lasers, respectively. The laser power for the Argon-ion and Helium-Neon Lasers was set to be 6.25 and 5 μW, respectively, for all experiments. This power level is high enough to observe the fluorescence signal form each molecule and still low enough to keep photobleaching negligible. The confocal pinhole diameters were adjusted to 70 μm for 488 nm and 90 μm for 633 nm laser lines, respectively. The emission signals were split through a dichroic mirror (570 nm beam splitter) and detected with a band-pass filter (505-550 nm) and a long-pass filter (650 nm) for green and red fluorescence, respectively. The confocal detection volume was ~ 0.2 fl. A glass-bottom 96-well plate (Whatman, Kent, England) was used as a sample chamber, and all measurements were performed in a sample volume of 100 μl. Samples adjusted to a protein concentration approximately 500 nM ~ 1 μM in high salt buffer with 2.2 mM $MgCl_2$ were diluted 10-fold with a buffer to the appropriate salt concentration, and incubated for 1 h on ice. For measurement of single species, the concentration of rod fragment used was approximately 100 nM. For measurement of the dual-species mixture, the concentration of each rod fragment used was approximately 50 nM. All measurements were performed at 25 °C. Each sample was measured for 30 sec, three times.

Auto- and cross-correlation curves obtained from FCS and FCCS measurements allow the determination of the particle number and the diffusion time of single color molecules as well as

the particle number of dual-color molecules, respectively (*35*). Mathematically, a correlation function $G(\tau)$ is defined as follows:

$$G_x(\tau) = \frac{< \delta I_\alpha(t) \cdot \delta I_\beta(t+\tau) >}{< I_\alpha(t) >< I_\beta(t) >} \quad , \qquad (1)$$

where τ is a lag time for correlation function. $I_\alpha(t)$ and $I_\beta(t)$ are time-dependent fluorescence intensity in the red channel ($\alpha = \beta = r$) or the green channel ($\alpha = \beta = g$), respectively, $G_x(\tau)$ denotes a correlation function calculated from fluctuations of the fluorescence intensity in red ($G_r(\tau)$; $\alpha = \beta = x = r$), green ($G_g(\tau)$; $\alpha = \beta = x = g$), and overlapping volume ($G_c(\tau)$; $\alpha = r$, $\beta = g$, and $x = c$), respectively. Acquired auto- and cross-correlation curves $G(\tau)$ were fitted with a one-, or a two-component model as follows:

$$G(\tau) = \left(1 + \frac{F_{trip}}{1 - F_{trip}} \cdot e^{-\tau / \tau_{trip}}\right) \cdot \frac{1}{N} \cdot \sum_i F_i \left(1 + \frac{\tau}{\tau_i}\right)^{-1} \left(1 + \frac{\tau}{s^2 \tau_i}\right)^{-1/2} + 1, \qquad (2)$$

where F_i and τ_i are the fraction and the diffusion time of component i^{th}, respectively. F_{trip} and τ_{trip} are a fraction and the time of triplet owing to the internal intensity fluctuations of fluorescent dye, respectively. Upon fitting a cross-correlation curve with the equation 2, F_{trip} was set to be zero since internal intensity fluctuations of individual dyes does not contribute to cross-correlation curve. N is the average number of fluorescent particles in the confocal volume element defined by the radius w_0 and length $2z_0$, s is the structure parameter representing the ratio, $s = z_0/w_0$. To compare the diffusion properties, autocorrelation curves were normalized by N. The average numbers of red fluorescent particles (N_r), green fluorescent particles (N_g), and particles that have both red and green fluorescence (N_c) can be calculated by

$$N_r = \frac{1}{G_r(0)}, \quad N_g = \frac{1}{G_g(0)}, \text{ and } N_c = \frac{G_c(0)}{G_r(0) \cdot G_g(0)}, \qquad (3)$$

respectively. When N_r and N_g are constant, $G_c(0)$ is directly proportional to N_c.

Diffusion coefficients of samples (D_{sample}) were calculated from the diffusion coefficient of standard fluorophores (D_{standard}), Rhodamine 6G ($D = 2.80 \times 10^{-6}$ cm^2/s) or Cy5 ($D = 3.16 \times 10^{-6}$ cm^2/s) (*36*), and diffusion times τ_{standard} and τ_{sample} with the following equation:

$$\frac{D_{sample}}{D_{standard}} = \frac{\tau_{standard}}{\tau_{sample}}. \quad (4)$$

Results

Assembly-Disassembly States of ARF and BRF Assessed by FCS

Myosin II rod fragments similar to myosin II molecules assemble into filaments at low ionic strength and the filaments disassemble at high ionic strength through mainly their electrostatic interaction (*4, 5, 7, 22, 37*). First, we assessed whether the assembled and disassembled states of the rod fragments can be distinguished by FCS method. Figures 1A and 1B show the autocorrelation curves of Alexa Fluor 633-labeled ARF296 (633-ARF) and Alexa Fluor 488-labeled BRF305 (488-BRF), respectively, obtained by FCS measurements at 500 mM NaCl (disassembled condition) or 50 mM NaCl (assembled condition). The correlation curves at 50 mM NaCl obviously shifted to the right direction compared to those at 500 mM NaCl in both 633-ARF and 488-BRF. These results indicate that FCS method can distinguish between the assembled and disassembled states of myosin II rod fragments. To obtain the diffusion time, the correlation curves were fitted by using the two-component model (i = 2 in equation 2) with the triplet component (for example, see Figure S1). The diffusion coefficients were calculated using equation 4. The diffusion coefficients of both 633-ARF and 488-BRF under the assembled condition (50 mM NaCl) were smaller than those under the disassembled condition (500 mM NaCl) (Table I), indicating that the fluorescent rod fragments became bigger due to the formation of assembly. Moreover, the diffusion coefficients obtained at 50 mM NaCl were comparable between 633-ARF and 488-BRF, nearly one third of those at 500 mM NaCl, suggesting a relatively stable size of homo-assembly was formed from the homogeneous C-terminal rod fragment of each isoform in the solution. Since the formed assemblies would most likely be rod-like shape with a side by side arrangement of the rod fragments (*3*), the observed three-fold difference of diffusion coefficients would not simply reflect the assembly as a trimer of the rod fragment, but probably reflect an entity with much more rod fragments.

Assembly-Mode of ARF and BRF Mixture Formed by Dilution Procedure

Next, we mixed 633-ARF and 488-BRF at 500 mM NaCl (disassembled condition) and then diluted them to 50 mM NaCl (assembled condition). FCS was performed on the resulting sample. The calculated diffusion coefficients of the mixture of 633-ARF and 488-BRF were comparable to the values obtained from the measurements of each isoform separately (Table I). This result indicates that the resulting assembly from the mixture by dilution procedure has a similar size to the homo-assemblies from each isoform. However, by the FCS method, we are not able to discriminate whether the resulting assembly is a homo-assembly that 633-ARF or 488-BRF assembled separately, or a hetero-assembly that they assembled together regardless of isoform.

To reveal the assembly mode, we performed FCCS analysis that is suitable for the measurement of the complexes labeled with spectrally separated probes, Alexa Fluor 633 and 488 in this study. The mixtures of 633-ARF and 488-BRF at various NaCl concentrations were measured by FCCS (Figure 2A). The cross-correlation signal was not observed under the disassembled condition (500 mM NaCl, closed square), but it was observed under the assembled condition (50 mM NaCl, closed circle). The y-intercept of the cross-correlation curve, namely the amplitude of cross-correlation curve, reflects the number of dual-colored complexes in the sample. The amplitude increased with decreasing concentrations of NaCl. These results clearly demonstrate that 633-ARF and 488-BRF diffuse individually at 500 mM NaCl and associate to form hetero-assemblies by the dilution procedure. Therefore, it appears that ARF and BRF assemble without any distinction between isoforms in vitro.

Assembling Properties of ARF and BRF in hetero-assemblies

To reveal whether the assembling property of one isoform is affected by another isoform, we analyzed the properties of each isoform in the hetero-assembly as well as in the homo-assembly by FCCS. To examine the properties in the homo-assembly, the fragments of one isoform were labeled with two different colors of fluorophore and mixed at 500 mM NaCl, and then the mixture was subjected to FCCS analysis at various NaCl concentrations (ARF, Figure 2B; BRF, Figure 2C). The amplitude of the cross-correlation curve increased with decreasing concentrations of

NaCl, indicating that the dual-colored homo-assemblies of one isoform were formed in a salt-dependent manner. To analyze quantitatively the assembling ability of rod fragments, we estimated the assembled fraction of rod fragments as a function of NaCl concentration using the amplitude of the FCCS data (Figure 2D). The assembled fractions of BRF alone (Figure 2D, closed circles) and ARF alone (Figure 2D, opened circles) decreased with an increase in the concentration of NaCl. BRF appeared to be in assemble state more than ARF under the conditions between 100 and 200 mM NaCl, indicating that ARF tends to be more soluble than BRF. This assembling tendency of each isoform was agreed with the previous results obtained by centrifugation method (*7, 22, 37*). The assembling ability of the rod fragments in the mixture of ARF and BRF showed a similar aspect to those showed by the dual-colored each isoform alone. It is noted that the assembled fractions from the mixture of ARF and BRF positioned between those of ARF and BRF alone at 150 and 200 mM NaCl, (Figure 2D, opened diamonds).

During the FCCS measurements, FCS data of each colored sample are obtained simultaneously. To clarify the effect of one isoform in the hetero-assembly on the assemble/disassemble state of another isoform, we estimated the assembled fraction of each isoform from the FCS data. The fluorescence autocorrelation curve at each condition was fitted to a two-component model (i = 2 in equation 2) with the fixed diffusion times for each of the fast- and slow-moving particles reflecting the disassembled and assembled molecules, respectively. As shown in Figures 2E and 2F, the properties of assembling ability of ARF and BRF were exhibited in an isoform-dependent manner, regardless of the experimental conditions. Taking into consideration of the difference in the brightness of fluorescence between monomer and assembly as suggested by Krouglova *et al*. (*38*), we corrected the ratio of assembled fraction as described in Supplemental information. The corrected results showed that the tendency of assembling properties of ARF and BRF was not changed from the original results (Figure S2). These results indicate that the salt-dependent assembling ability of ARF or BRF is not due to the assembling species, hetero-assembly or homo-assembly. In other words, the assembling properties of one

isoform in hetero-assembly could not be affected by the presence of another isoform during the salt-dependent assembling process.

Stability of Assembly of the Rod Fragments

Next, we assessed whether the homo-assemblies formed once are stable or not. After the homo-assemblies of 633-ARF and 488-BRF were formed separately at 50 mM NaCl, they were mixed together, and the time-course of the cross-correlation functions was monitored (Figure 3). The cross-correlation amplitudes increased with the passage of time and reached a plateau within 20 min after mixing, indicating the hetero-assemblies were formed quickly. There are two possible modes of formation of hetero-assembly. First, each pre-formed homo-assemblies consisting of 633-ARF and 488-BRF just associate, so that relatively large hetero-assemblies are formed. Second, the rod fragments exist in an equilibrium state between assemblies and monomers even under the assembled condition (50 mM NaCl), so that the rod fragments transiently dissociated from each homo-assemblies re-associate to form hetero-assemblies. The latter is probably the most likely, because the diffusion coefficient of hetero-assemblies (0.81 ± 0.09 [$\times 10^{-7}$ cm^2/s]) at 30 min after mixing pre-formed homo-assemblies was equivalent to that of the homo-assemblies formed by dilution procedure (633-ARF, 0.80 ± 0.07 [$\times 10^{-7}$ cm^2/s]; 488-BRF, 0.81 ± 0.04 [$\times 10^{-7}$ cm^2/s]; Table I). These results demonstrate that the homo-assemblies of each isoform are not stable, and the exchange of the rod fragments among the assemblies occurs quickly. That is, the rod fragments dissociated from the homo-assemblies once can associate randomly with either assemblies and the exchange reaction came to equilibrium within 20 min.

Dynamic assembly-disassembly properties induced by Mts1

We examined the effects of Mts1 on the assembly mode of rod fragments, because Mts1 binds to ARF specifically and causes ARF to disassemble in a Ca^{2+}-dependent manner (*22, 28*). We first investigated each of the homo-assemblies in the presence or absence of Mts1 by FCS

measurement (Figure 4). The autocorrelation curve under the assembled condition even with 0.2 mM $CaCl_2$ was similar to that at 50 mM NaCl without $CaCl_2$ (Figure 1, closed circles; Figure 4, closed triangles). By the addition of 5 μM Mts1 to the same chamber, the autocorrelation curve of 633-ARF shifted to the left (Figure 4A, closed circles), but that of 488-BRF did not (Figure 4B, closed circles). The diffusion coefficient of 633-ARF in the presence of Mts1 (3.02 ± 0.03 [$\times 10^{-7}$ cm^2/s]) was almost comparable to that under the disassembled condition (2.61 ± 0.08 [$\times 10^{-7}$ cm^2/s]) (Tables I and II). These results indicate that Mts1 selectively affects ARF and keep it disassembled. Following addition of 1 mM EGTA to the same chamber for chelating Ca^{2+}, the autocorrelation curve of 633-ARF returned to the form comparable to the original one (Figure 4A, open circles). In contrast, no change was observed in autocorrelation curve of 488-BRF by the addition of EGTA (Figure 4B, open circles). These results clearly indicate that Mts1 controls the assembly mode of ARF specifically, supporting the previously reported results (*22*, *28*).

Next, we investigated whether Mts1 can distinguish ARF from BRF in the hetero-assemblies. We performed FCCS measurement of the mixture of 633-ARF and 488-BRF in the presence or absence of Mts1 (Figure 5). Cross-correlation signal was observed under the assembled condition with 0.2 mM $CaCl_2$ (Figure 5A, closed triangles) and disappeared following addition of 5 μM Mts1 (Figure 5A, closed circles). The simultaneously recorded autocorrelation curve of 633-ARF shifted to the left following addition of Mts1 (Figure 5B, closed circles), but that of 488-BRF did not change remarkably (Figure 5C, closed circles). These results indicate that the addition of Mts1 specifically makes ARF disassemble from the hetero-assemblies and prevents the transiently dissociated ARF monomer from re-assembling, and consequently forms homo-assemblies of BRF with a similar size to the original hetero-assemblies. After addition of 1 mM EGTA to chelate Ca^{2+}, the cross-correlation signal reappeared (Figure 5A, open circles) and the autocorrelation curve of 633-ARF shifted back to the curve similar to the original one (Figure 5B, open circles), but that of 488-BRF did not change (Figure 5C, open circles). These results indicate that Mts1 dissociates from the ARF monomer under low Ca^{2+} conditions, and then the

free ARF monomer replaces BRF to reconstruct hetero-assemblies. A simple schematic model of this process is shown in Figure 6.

Discussion

In this study, we analyzed the assembly properties of nonmuscle myosin II isoform rod fragments by FCS and FCCS. The results demonstrated that hetero-assemblies were formed from a mixture of myosin IIA and IIB rod fragments, and that the exchange reaction of subunits (rod fragments) proceeded quickly among the assemblies in an isoform-independent manner. Through the combination of FCS and FCCS methods, which enables us to acquire information on both the interaction of molecules and the size of each molecule simultaneously, we also showed dynamic effects of Mts1 against hetero-assemblies of myosin II rod fragments.

We have assumed that the nonhelical tailpieces of each isoform play a role in distinguishing their own isoform from others to form homo-filaments, because of their significant differences in primary structures. However, Murakami *et al*. reported that the rod fragments of myosin IIA and IIB (longer than our present fragments) coassembled *in vitro* as judged by solubility analysis using centrifugation (*22*). We initially expected that the formation of homo-assemblies could be detected directly by FCS and FCCS analyses of individual assembling particles. However, contrary to the expectation, we detected the formation of hetero-assemblies by FCCS (Figure 2), even in the case of the mixture of the pre-formed ARF and BRF homo-assemblies (Figure 3). Thus, we confirmed the results of Murakami *et al*. by using the experiments down to the single-molecule level.

We demonstrated here that dynamic exchange of subunits between the assemblies of rod fragments could be detected by FCCS. The reaction came to equilibrium within 20 min (Figure 3). The phenomenon of subunit exchange between filaments was observed in the case of skeletal muscle myosin by a fluorescence resonance energy transfer (FRET) assay (*39*) and in smooth muscle myosin by an electron microscopic observation (*40*). They demonstrated the exchange of subunit using one species of myosin II molecules. We demonstrated here that the exchange could occur between the different isoforms of nonmuscle myosin II fragments. The times to reach equilibrium were approximately 15 min in both cases of skeletal and smooth muscle myosins (*39, 40*). The exchange speed of the rod fragments in this study was comparable to those of other

myosins, indicating that the rod fragments retain the assembly property of full length of nonmuscle myosin II. Dynamic exchange of subunits among filaments would be associated with the dynamic assembly-disassembly transitions of the myosin II molecule. Myosin II dissociated from one filament would enter into another filament. The results shown here suggest that the rod fragments undergo this process without distinction between ARF and BRF *in vitro*.

The assembling properties of the rod fragments in this study showed some discrepancies with the results using a centrifugation method (*7, 22*). Firstly, the assembling abilities of the rod fragments in this study were lower than previous studies around physiological salt concentrations. Secondly, Murakami *et al*. reported that Mts1 did not solubilize the IIA rod fragments at low salt conditions such as 50 mM NaCl (*22*), but Mts1 solubilized ARFs at 50 mM NaCl in this study. These discrepancies might be caused by the difference in protein concentration used for the assays. The previous studies used 2.1 μM (*22*) and 1.7 μM (*7*) of the rod fragments, respectively, whereas we used 100 nM of them in this study. Although the exact concentration of myosin II at a certain region in the cell is not determined, the average concentrations of nonmuscle myosin II were estimated to be in the range of about 20 nM (erythrocytes) (*41*) to 2 μM (platelets) (*42*). We might observe the behavior of myosin II molecules in the condition corresponding to the region, where the concentration of myosin II is relatively low in a cell, by FCS and FCCS. Thirdly, Murakami *et al*. demonstrated that the properties of salt-dependent solubility of IIA and IIB rod fragments became similar to each other when they were mixed together (*22*). However, in this study, each isoform exhibited the salt-dependent solubility in an isoform-dependent manner. That is, ARF was more soluble than BRF, regardless of the mode of assemblies (homo- or hetero-) (Figure 2E and 2F). This discrepancy may be due to difference in the method to analyze the assembly state of the rod fragments. Because FCS and FCCS are not subjected to centrifugal force load, these methods might detect the more delicate assembly-disassembly processes.

It was suggested by *in vitro* studies that the assembly of each isoform was regulated by a distinct mechanism through the C-terminal end region including the nonhelical tailpiece, that is,

phosphorylation by protein kinase C for IIB (*22, 37, 43*) and Mts1 binding for IIA (*22, 28, 44*). It was demonstrated that Mts1 inhibits assembly of IIA rod fragments selectively when a mixture of IIA and IIB rod fragments monomers was studied under conditions favoring to assembly (*22*). In the present study, we showed that Mts1 allowed ARF to disassemble from pre-formed hetero-assemblies of ARF and BRF. The disappearance of the cross-correlation signal by the addition of Mts1 was very fast (less than 30 sec) (data not shown). If Mts1 binds to the ARF monomer that dissociated from the hetero-assembly during the dynamic assembly-disassembly process and prevents ARF monomer from reentering assembly, the rate of disappearance of the cross-correlation signal would be close to 20 min. Mts1 would be able to strip ARF away from the hetero-assembly and keep it in the disassembled-form. Figure 5 shows that BRFs keep the assembled state during the dynamic change in the ARF state by Mts1. Once hetero-filaments are formed somewhere in a cell, a factor like Mts1 may specifically remove one isoform from the hetero-filaments and make homo-filaments of another isoform.

It was shown that Mts1 was localized to the posterior region of migrating cells (*45*), where myosin IIA was present but myosin IIB was not (*20, 21*). FRET experiments demonstrated the direct association of a C-terminal rod fragment of the myosin IIA heavy chain with Mts1 in living cells (*46*). It was also suggested that this interaction with myosin IIA is important for Mts1's ability to induce the metastatic phenotype (*47, 48*). These observations strongly imply that the interaction of myosin IIA with Mts1 in the leading edge of migrating cell would be essential for metastasis. Furthermore, it was demonstrated that Mts1 binding inhibits phosphorylation of heavy chain IIA at Ser 1917 within the Mts1 binding site or at Ser 1944 in the nonhelical tailpiece (*28, 49*). It was also demonstrated that phosphorylation of Ser 1944 by casein kinase 2 decreased the affinity of Mts1 for IIA rod fragment (*49*). The C-terminal region including the Mts1-binding site as well as the nonhelical tailpiece could be responsible for regulating myosin II assembly in an isoform-specific manner.

It was reported that the subcellular localization of myosin IIA and IIB depends on their rod-like tail region instead of their head region (*50, 51*). In particular, it was indicated that the

C-terminal end regions were required for the isoform-specific localization (*51*) as well as the assembly of myosin II molecules in the cell (*51-54*). We have found that exogenous expression of BRF305 in the cells induced an unstable cell shape similar to MHC-IIB$^{-/-}$ fibroblasts, and demonstrated this dominant negative effect was caused in an isoform-specific manner (*33*). The recognition of oneself by C-terminal region of each isoform might require certain post-translational modifications or the interaction of some factors. It is possible that myosin IIA and IIB form the respective homo-filaments by some unknown mechanism in a living cell.

Recently, Beach and Egelhoff suggested that myosin IIA and IIB co-assemble to form hetero-filaments in the contractile ring (*55*). It is an important issue whether myosin II isoforms to form homo- or hetero-filaments at the region besides a contractile ring in the cell. As FCS and FCCS are approaches basically consisting of noninvasive procedures, we believe that these measurements in a living cell can contribute to the study of the dynamic assembly properties of nonmuscle myosin II molecules and their interaction with other regulatory proteins in future.

Acknowledgements

We thank Dr. R. S. Adelstein (National Heart, Lung, and Blood Institute, National Institutes of Health, Bethesda, MD, USA) for his helpful discussion and critical reading of the manuscript. We also thank Dr. M. Tamura and Dr. Y. Murakami for valuable discussion, Dr. S. Kaya for the DNA sequencer, and Dr. A. Nakatomi, Dr. T. Nakasawa, Dr. M. K. Sato Ms. Y. Hirayama (Hokkaido University, Sapporo, Japan) for technical assistance and valuable discussion. This work was supported by Grants-in-Aid for Scientific Research (C) 18570144 and 22570129 from the Japan Society for the Promotion of Science.

References

1. Sellers, J.R. (1999) Myosins. 2nd Ed. Oxford University Press, Oxford, U.K.

2. Krendel M. and Moosker, M.S. (2005) Myosins: Tails (and heads) of functional diversity. *Physiology* **20**, 239-251

3. Craig, R. and Woodhead, J.L. (2006) Structure and function of myosin filaments. *Curr. Opin. Struct. Biol.* **16**, 204-212

4. Hodge, T.P., Cross, R., and Kendrick-Jones, J. (1992) Role of the COOH-terminal nonhelical tailpiece in the assembly of a vertebrate nonmuscle myosin rod. *J. Cell Biol.* **118**, 1085-1095

5. Sohn, R.L., Vikstrom, K.L., Strauss, M., Cohen, C., Szent-Györgyi, A.G., and Leinwand, L.A. (1997) A 29 residue region of the sarcomeric myosin rod is necessary for filament formation. *J. Mol. Biol.* **266**, 317-330

6. Ikebe, M., Komatsu, S., Woodhead, J. L., Mabuchi, K., Ikebe, R., Saito, J., Craig, R., and Higashihara, M. (2001) The tip of the coiled-coil rod determines the filament formation of smooth muscle and nonmuscle myosin, *J. Biol. Chem.* **276**, 30293-30300.

7. Nakasawa, T., Takahashi, M., Matsuzawa, F., Aikawa, S., Togashi, Y., Saitoh, T., Yamagishi, A., and Yazawa, M. (2005) Critical regions for assembly of vertebrate nonmuscle myosin II. *Biochemistry* **44**, 174-183

8. Conti, M.A. and Adelstein R.S. (2008) Nonmuscle myosin II moves in new directions. *J. Cell Sci.* **121**, 11-18

9. Vicente-Manzanares, M., Ma, X., Adelstein, R.S., and Horwitz, A.R. (2009) Non-muscle myosin II takes centre stage in cell adhesion and migration. *Nature Rev. Mol Cell Biol.* **10**, 778-790

10. Shohet, R.V., Conti, M.A. Kawamoto, S., Preston, Y.A., Brill, D.A., and Adelstein, R.S. (1989) Cloning of the cDNA encoding the myosin heavy chain of a vertebrate cellular myosin. *Proc. Natl. Acad. Sci. USA* **86**, 7726-7730

11. Takahashi, M., Kawamoto, S., and Adelstein, R.S. (1992) Evidence for inserted sequences in the head region of nonmuscle myosin specific to the nervous system. Cloning of the cDNA encoding the myosin heavy chain-B isoform of vertebrate nonmuscle myosin. *J. Biol. Chem*. **267**, 17864-17871

12. Berg, J.S., Powell, B.C., and Cheney, R.E. (2001) A millennial myosin census. *Mol. Biol. Cell* **12**, 780-94

13. Golomb, E., Ma, X., Jana, S.S., Preston, Y.A., Kawamoto, S., Shoham, N.G., Goldin, E., Conti, M.A., Sellers, J.R., and Adelstein, R.S. (2004) Identification and characterization of nonmuscle myosin II-C. A new member of the myosin II family. *J. Biol. Chem.* **279**, 2800-2808

14. Wang, F., Kovacs, M., Hu, A., Limouze, J., Harvey, E.V., and Sellers, J.R. (2003) Kinetic mechanism of non-muscle myosin IIB. Functional adaptations for tension generation and maintenance. *J. Biol. Chem*. **278**, 27439-27448

15. Kovacs, M., Wang, F., Hu, A., Zhang, Y., and Sellers, J.R. (2003) Functional divergence of human cytoplasmic myosin II. Kinetic characterization of the non-muscle IIA isoform. *J. Biol. Chem*. **278**, 38132-38140

16. Tullio, A.N., Accili, D., Ferrans, V.J., Yu, Z., Takeda, K., Grinberg, A., Westphal, H., Preston, Y.A., and Adelstein, R.S. (1997) Nonmuscle myosin II-B is required for normal development of the mouse heart. *Proc. Natl. Acad. Sci. USA* **94**, 12407-12412

17. Lo, C.M., Buxton, D.B. Chua, G.C. Dembo, M., Adelstein, R.S., and Wang, Y.L. (2004) Nonmuscle myosin IIB is involved in the guidance of fibroblast migration. *Mol. Biol. Cell* **15**, 982-989

18. Conti, M.A., Even-Ram, S., Liu, C., Yamada, K.M., and Adelstein, R.S. (2004) Defects in cell adhesion and the visceral endoderm following ablation of nonmuscle myosin heavy chain II-A in mice. *J. Biol. Chem.* **279**, 41263-41266

19. Maupin, P., Phillips, C.L., Adelstein, R.S., and Pollard, T. D. (1994) Differential localization of myosin-II isozymes in human cultured cells and blood cells. *J. Cell Sci.* **107**, 3077-3090

20. Saitoh, T., Takemura, S., Ueda, K., Hosoya, H., Nagayama, M., Haga, H., Kawabata, K., Yamagishi, A., and Takahashi, M. (2001) Differential localization of non-muscle myosin II isoforms and phosphorylated regulatory light chains in human MRC-5 fibroblasts. *FEBS Lett*. **509**, 365-369

21. Kolega, J. (2003) Asymmetric distribution of myosin IIB in migrating endothelial cells is regulated by a rho-dependent kinase and contributes to tail retraction. *Mol. Biol. Cell* **14**, 4745-4757

22. Murakami, N., Kotula, L., and Hwang, Y.W. (2000) Two distinct mechanisms for regulation of nonmuscle myosin assembly via the heavy chain: Phosphorylation for MIIB and Mts 1 binding for MIIA. *Biochemistry* **39**, 11441-11451

23. Ebralidze, A., Tulchinsky, E., Grigorian, M., Afanasyeva, A., Senin, V., Revazova, E., and Lukanidin, E. (1989) Isolation and characterization of a gene specifically expressed in different metastatic cells and whose deduced gene product has a high degree of homology to a Ca^{2+}-binding protein family. *Genes Dev*. **3**, 1086-1093

24. Garrett, S.C., Varney, K.M., Weber, D.J., and Bresnick, A.R. (2006) S100A4, a mediator of metastasis. J. *Biol. Chem*. **281**, 677-680

25. Kriajevska, M.V., Cardenas, M.N., Grigorian, M.S., Ambartsumian, N.S., Georgiev, G.P., and Lukanidin, E.M. (1994) Non-muscle myosin heavy chain as a possible target for protein encoded by metastasis-related *mts-1* Gene. *J. Biol. Chem*. **269**, 19679-19682

26. Ford, H.L. and Zain, S.B. (1995) Interaction of metastasis associated Mts1 protein with nonmuscle myosin. *Oncogene* **10**, 1597-1605

27. Kriajevska, M., Tarabykina, S., Bronstein, I., Maitland, N., Lomonosov, M., Hansen, K., Georgiev, G., and Lukanidin, E. (1998) Metastasis-associated Mts1 (S100A4) protein modulates protein kinase C phosphorylation of the heavy chain of nonmuscle myosin. *J. Biol. Chem*. **273**, 9852-9856

28. Li, Z.H., Spektor, A., Varlamova, O., and Bresnick, A.R. (2003) Mts1 regulates the assembly of nonmuscle myosin-IIA. *Biochemistry* **42**, 14258-14266

29. Rigler, R., Mets, U., Widengren, J., and Kask, P. (1993) Fluorescence correlation spectroscopy with high count rate and low background: analysis of translational diffusion. *Eur. Biophys. J*. **22**, 169-175

30. Kinjo, M. and Rigler, R. (1995) Ultrasensitive hybridization analysis using fluorescence correlation spectroscopy. *Nucleic Acids Res*. **23**, 1795-1799

31. Schwille, P. (2001) Cross-correlation analysis in FCS. In Fluorescence Correlation Spectroscopy: Theory and Applications (Rigler, R. and Elson, E. L. Ed.,) pp. 360-678. Springer-Verlag, Berlin.

32. Thompson, N.L., Lieto, A.M., and Allen, N.W. (2002) Recent advances in fluorescence correlation spectroscopy. *Curr. Opin. Struct. Biol.* **12**, 634-641

33. Sato, M.K., Takahashi, M., and Yazawa, M. (2007) Two regions of the tail are necessary for the isoform-specific functions of nonmuscle myosin IIB. *Mol. Biol. Cell* **18**, 1009-1017

34. Weiner, M.P., Costa, G.L., Schoettlin, W., Cline, J., Mathur, E., and Bauer, J.C. (1994) Site-directed mutagenesis of double-stranded DNA by the polymerase chain reaction. *Gene* **151**, 119-123

35. Saito, K., Wada, I., Tamura, M., and Kinjo, M. (2004) Direct detection of capase-3 activation in single live cells by cross-correlation analysis. *Biochem. Biophys. Res. Commun.* **324**, 849-854

36. Weisshart, K., Jüngel, V., and Briddon, S.J. (2004) The LSM 510 META – ConfoCor 2 system: An integrated imaging and spectroscopic platform for single-molecule detection. *Curr. Pharm. Biotechnol*. **5**, 135-154

37. Murakami, N., Singh, S.S., Chauhan, V.P.S., and Elzinga, M. (1995) Phospholipid binding, phosphorylation by protein kinase C, and filament assembly of the COOH terminal heavy chain fragments of nonmuscle myosin II isoforms MIIA and MIIB. *Biochemistry* **34**, 16046-16055

38. Krouglova, T., Vercammen, J., and Engelborghs, Y. (2004) Correct diffusion coefficients of proteins in fluorescence correlation spectroscopy. Application to tubulin oligomers induced by Mg^{2+} and paclitaxel. *Biophys. J.* **87**, 2635-2646

39. Saad, A.D., Pardee, J.D., and Fischman, D.A. (1986) Dynamic exchange of myosin molecules between thick filaments. *Proc. Natl. Acad. Sci. USA* **83**, 9483-9487

40. Trybus, K.M. and Lowey, S. (1987) Subunit exchange between smooth muscle myosin filaments. *J Cell Biol*. **105**, 3021-3030

41. Wong, A.J., Kiehart, D.P., and Pollard, T.D. (1985) Myosin from human erythrocytes. *J. Biol. Chem*. **260**, 46-49

42. Pollard, T.D., Thomas, S.M., and Niederman, R. (1974) Human platelet myosin. I. Purification by a rapid method applicable to other nonmuscle cells. *Anal. Biochem.* **60**, 258-266

43. Rosenberg, M. and Ravid S. (2006) Protein kinase Cγ regulates myosin IIB phosphorylation, cellular localization, and filament assembly. *Mol. Biol. Cell* **17**, 1364-1374

44. Dulyaninova, N.G., Malashkevich, V.N., Almo, S.C., and Bresnick, A.R. (2005) Regulation of myosin-IIA assembly and Mts1 binding by heavy chain phosphorylation. *Biochemistry* **44**, 6867-6876

45. Kim, E.J. and Helfman, D.M. (2003) Characterization of the metastasis-associated protein, S100A4. Roles of calcium binding and dimerization in cellular localization and interaction with myosin. *J. Biol. Chem*. **278**, 30063-30073

46. Zhang, S., Wang, G., Fernig, D.G., Rudland, P.S., Webb, S.E.D., Barraclough, R., and Martin-Fernandez, M. (2005) Interaction of metastasis-inducing S100A4 protein *in vivo* by fluorescence lifetime imaging microscopy. *Eur. Biophys. J.* **34**, 19-27

47. Wang, G., Zhang, S., Fernig, D.G., Martin-Fernandez, M., Rudland, P.S., and Barraclough, R. (2005) Mutually antagonistic actions of S100A4 and S100A1 on normal and metastatic phenotypes. *Oncogene* **24**, 1445-1454

48. Zhang, S., Wang, G., Liu, D., Bao, Z., Fernig, D.G., Rudland, P.S., and Barraclough, R. (2005) The C-terminal region of S100A4 is important for its metastasis-induced properties. *Oncogene* **24**, 4401-4411

49. Kriajevska, M., Igor, B., Scott, D.J., Tarabykina, S., Fischer-Larsen, M., Issinger, O-G., and Lukanidin, E. (2000) Metastasis-associated protein Mts1 (S100A4) inhibits

CK2-mediated phosphorylation and self-assembly of the heavy chain of nonmuscle myosin. *Biochim. Biophys. Acta* **1498**, 252-263

50. Vicente-Manzanares, M., Koach, M.A., Whitmore, L., Lamers, M.L., and Horwitz, A.F. (2008) Segregation and activation of myosin IIB creates a rear in migrating cells. *J. Cell Biol.* **183**, 543-55442.

51. Sandquist, J.C. and Means, A.R. (2008) The C-terminal tail region of nonmuscle myosin II directs isoform-specific distribution in migrating cells. *Mol. Biol. Cell* **19**, 5156-5167

52. Wei, Q. and Adelstein, R.S. (2000) Conditional expression of a truncated fragment of nonmuscle myosin II-A alters cell shape but not cytokinesis in HeLa cells. *Mol. Biol. Cell* **11**, 3617-3627

53. Rosenberg, M., Straussman, R., Ben-Ya'acov, A., Ronen, D., and Ravid, S. (2008) MHC-IIB filament assembly and cellular localization are governed by the rod net charge. *PLoS One* **3**, e1496

54. Breckenridge, M.T., Dulyaninova, N.G., Egelhoff, T.T. (2009) Multiple regulatory steps control mammalian nonmuscle myosin II assembly in live cells. *Mol. Biol. Cell* **20**, 338-347

55. Beach, J.R. and Egelhoff, T.T. (2009) Myosin II recruitment during cytokinesis independent of centralspindlin-mediated phosphorylation. *J. Biol. Chem.* **284**, 27377-27383

Table I. Diffusion coefficients of 633-ARF, 488-BRF and their mixture[a]

	Diffusion coefficients ($\times 10^{-7}$ cm^2/s)	
	[NaCl]	
	500 mM	50 mM
633-ARF	2.61 ± 0.08	0.80 ± 0.07
488-BRF	2.38 ± 0.11	0.81 ± 0.04
633-ARF + 488-BRF (488)[b]	2.53 ± 0.10	0.85 ± 0.10
633-ARF + 488-BRF (488)[c]		0.81 ± 0.09

[a]The values shown are means ± S. D. of three measurements. [b]The mixture prepared by the dilution procedure was analyzed by FCS using 488 nm laser line. [c]After 633-ARF and 488-BRF formed homo-assemblies separately at 50 mM NaCl, they were mixed together and the cross-correlation functions were measured after 30 min of incubation. The autocorrelation curve was analyzed using 488 nm laser lines. The diffusion coefficients were calculated from each autocorrelation curve with equations 2 and 4.

Table II. Diffusion coefficients of 633-ARF, 488-BRF and their mixture[a]

	Diffusion coefficients ($\times 10^{-7}$ cm^2/s)		
	+ Ca^{2+}		– Ca^{2+}
	– Mts1	+ Mts1	+ Mts1
633-ARF	0.79 ± 0.03	3.02 ± 0.03 [c]	0.73 ± 0.07
488-BRF	0.79 ± 0.03	0.82 ± 0.07	0.76 ± 0.05
633-ARF + 488-BRF (633)[b]	0.76 ± 0.05	3.14 ± 0.09 [c]	0.74 ± 0.06
633-ARF + 488-BRF (488)[b]	0.85 ± 0.05	0.79 ± 0.11	0.72 ± 0.07

[a]The values shown are means ± S. D. of three measurements. [b]The autocorrelation curves of the mixture analyzed using 633 nm or 488 nm laser lines. [c]The diffusion constants of 633-ARF with Mts1 in the presence of Ca^{2+} were a little larger than those without Mts1 ($2.61 \pm 0.08 \times 10^{-7}$ cm^2/s in Table I). This may indicate that the conformation of ARF-Mts1 complex is slightly more compact than that of ARF alone.

Figure Legends

Fig. 1 FCS measurements of 633-ARF and 488-BRF

Assembly-disassembly states of 633-ARF (A) and 488-BRF (B) were measured in 20 mM sodium phosphate (pH7.2) and 2 mM $MgCl_2$ with 50 mM NaCl (closed circle) or with 500 mM NaCl (open circle). The concentration of each rod fragment used was 100 nM. The autocorrelation curves obtained from FCS measurement were normalized at 0.012 ms for comparison of a lateral shift that indicates the changes on diffusion properties of target molecules. The obtained diffusion times of 633-ARF were 481 ± 19 μs and 1520 ± 110 μs at 500 mM and 50 mM NaCl, respectively (n = 3). The obtained diffusion times of 488-BRF were 338 ± 20 μs and 956 ± 58 μs at 500 mM and 50 mM NaCl, respectively (n = 3). Due to differences in confocal volumes of laser lines for 488 nm and 633 nm, the diffusion times of 488-BRF became smaller than those of 633-ARF, even though their diffusion coefficients were comparable.

Fig. 2 FCCS analyses of mixtures of rod fragments labeled with different fluorophores at various NaCl concentrations

Cross-correlation curves of mixtures of 633-ARF and 488-BRF (A), 633-ARF and 488-ARF (B) and 633-BRF and 488-BRF (C), respectively. Cross-correlation curves were measured in 20 mM sodium phosphate (pH7.2) and 2 mM $MgCl_2$ with the concentrations of NaCl indicated. The concentration of each rod fragment used was 50 nM. (D) Normalized amplitudes of cross-correlation curves of mixtures of rod fragments, 633-ARF and 488-ARF (open circle), 633-BRF and 488-BRF (closed circle), 633-ARF and 488-BRF (open diamond), as a function of NaCl concentration. Data represent mean + S. D. of three independent experiments. (E) Assembled fractions of 633-ARF in the mixture of 633-ARF and 488-ARF (open circle), 488-BRF in the mixture of 633-BRF and 488-BRF (closed circle) as a function of NaCl concentration estimated by fitting with the two-component model (i = 2 in equation 2). The diffusion times for the fast- (disassembled fragment at 500 mM NaCl) and slow- (assembled

fragments at 50 mM NaCl) components were adopted as two components. For 633-ARF, those of the fast and slow components were fixed to 481 μs and 1,520 μs, respectively. For 488-BRF, those of the fast and slow components were fixed 338 μs and 956 μs, respectively. Data represent mean + S. D. of three independent experiments. (F) Assembled fractions of 633-ARF (open diamond) and 488-BRF (closed diamond) in the mixture of 633-ARF and 488-BRF as a function of NaCl concentration estimated by fitting the two-component model.

Fig. 3 Cross-correlation curves of a mixture of pre-formed homo-assemblies

Cross-correlation curves were measured in 20 mM sodium phosphate (pH7.2) and 2 mM $MgCl_2$ with 50 mM NaCl at the times after mixing the pre-formed homo-assemblies of 633-ARF and 488-BRF. The concentration of each rod fragment used was 50 nM. 0.7 min (closed diamond), 1.5 min (open square), 7 min (closed square), 10 min (open triangle), 12 min (closed triangle), 20 min (open circle), 30 min (closed circle).

Fig. 4 Effect of Mts1 on homo-assemblies of 633-ARF and 488-BRF

Autocorrelation curves of 633-ARF (A) and 488-BRF (B) were measured in 20 mM sodium phosphate (pH7.2), 2 mM $MgCl_2$, 50 mM NaCl and 0.2 mM $CaCl_2$ (closed triangle), following addition of 5 μM Mts1 to the same chamber (closed circle), and following addition of 1 mM EGTA (open circle). The concentration of each rod fragment used was 100 nM. The autocorrelation curves were normalized at 0.012 ms. The calculated diffusion coefficients of 633-ARF and 488-BRF are shown in Table II.

Fig. 5 Effect of Mts1 on cross-correlation and autocorrelation curves of a mixture of 633-ARF and 488-BRF

Cross-correlation curves of a mixture of 633-ARF and 488-BRF (A) were measured in 20 mM sodium phosphate (pH7.2), 2 mM $MgCl_2$, 50 mM NaCl and 0.2 mM $CaCl_2$ (closed triangle), following addition of 5 μM Mts1 to the same chamber (closed circle), and further following addition of 1 mM EGTA (open circle). The concentration of each rod fragment used was 50 nM. Simultaneously, autocorrelation curves of each fragment, 633-ARF (B), 488-BRF (C), were recorded and normalized at 0.012 ms. The symbols are same to (A). The calculated diffusion coefficients of the mixture of 633-ARF and 488-BRF are shown in Table II.

Fig. 6 Schematic model of the dynamic assembly-disassembly process of a mixture of ARF and BRF regulated by Mts1 and Ca^{2+}

The rod fragments colored with dark and light gray indicate the BRF and ARF, respectively. White ellipses indicate Mts1. Small black circles indicate Ca^{2+}. In the absence of Ca^{2+}, hetero-assemblies consisting of ARF and BRF are formed even in the presence of Mts1. In the presence of Ca^{2+}, the Ca^{2+}-bound Mts1 dimers associate with ARF and keep ARF disassemble form, and consequently homo-assemblies of BRF are formed. This process is reversible.

Fig. 1

A

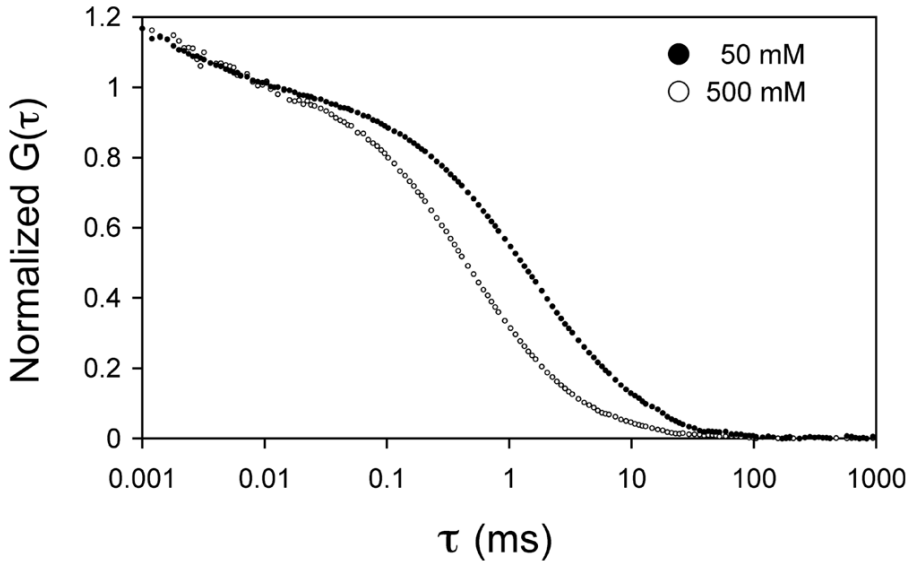
Normalized G(τ)
1.2
1
0.8
0.6
0.4
0.2
0
0.001
0.01
0.1
1
10
100
1000
τ (ms)
50 mM
500 mM

B

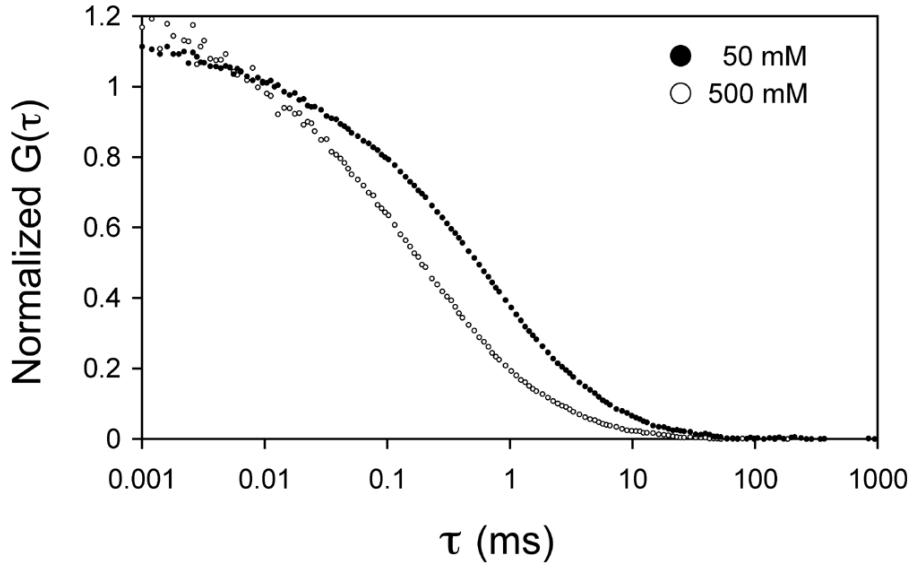
Normalized G(τ)
1.2
1
0.8
0.6
0.4
0.2
0
0.001
0.01
0.1
1
10
100
1000
τ (ms)
50 mM
500 mM

Fig. 2

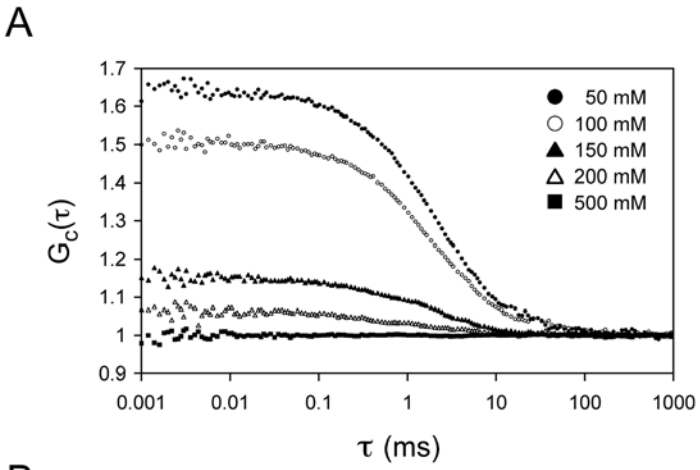
A
50 mM
100 mM
150 mM
200 mM
500 mM
$G_c(\tau)$
τ (ms)

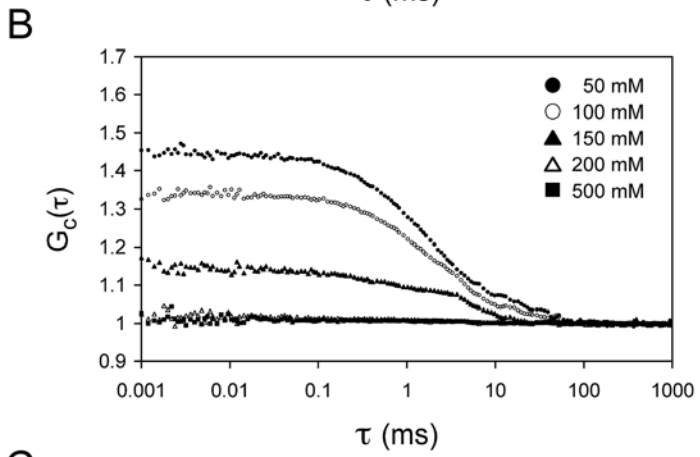
B
50 mM
100 mM
150 mM
200 mM
500 mM
$G_c(\tau)$
τ (ms)

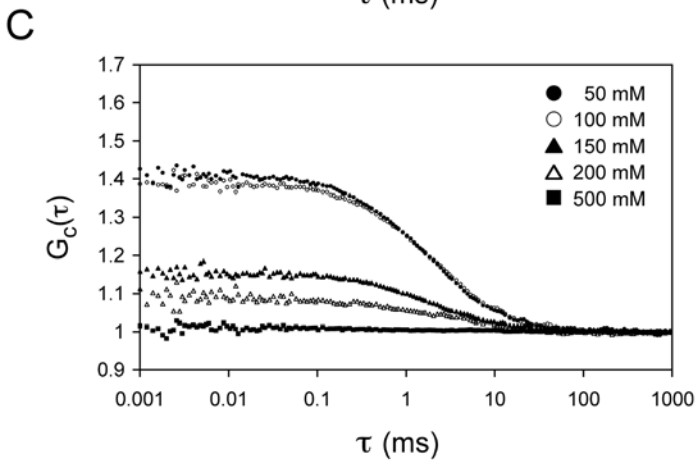
C
50 mM
100 mM
150 mM
200 mM
500 mM
$G_c(\tau)$
τ (ms)

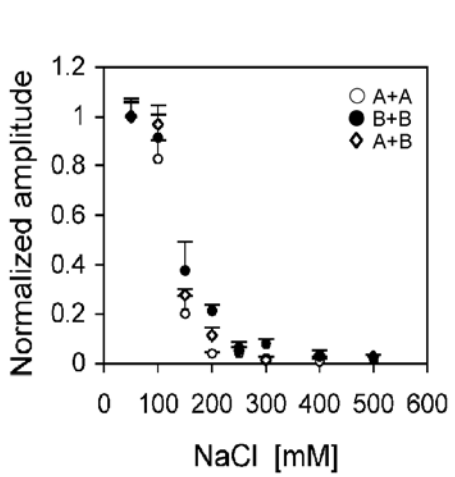
D
A+A
B+B
A+B
Normalized amplitude
NaCl [mM]

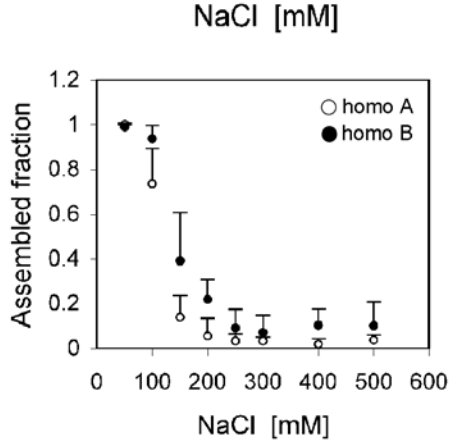
E
homo A
homo B
Assembled fraction
NaCl [mM]

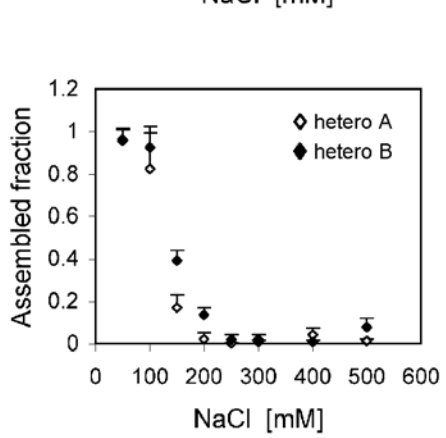
F
hetero A
hetero B
Assembled fraction
NaCl [mM]

Fig. 3

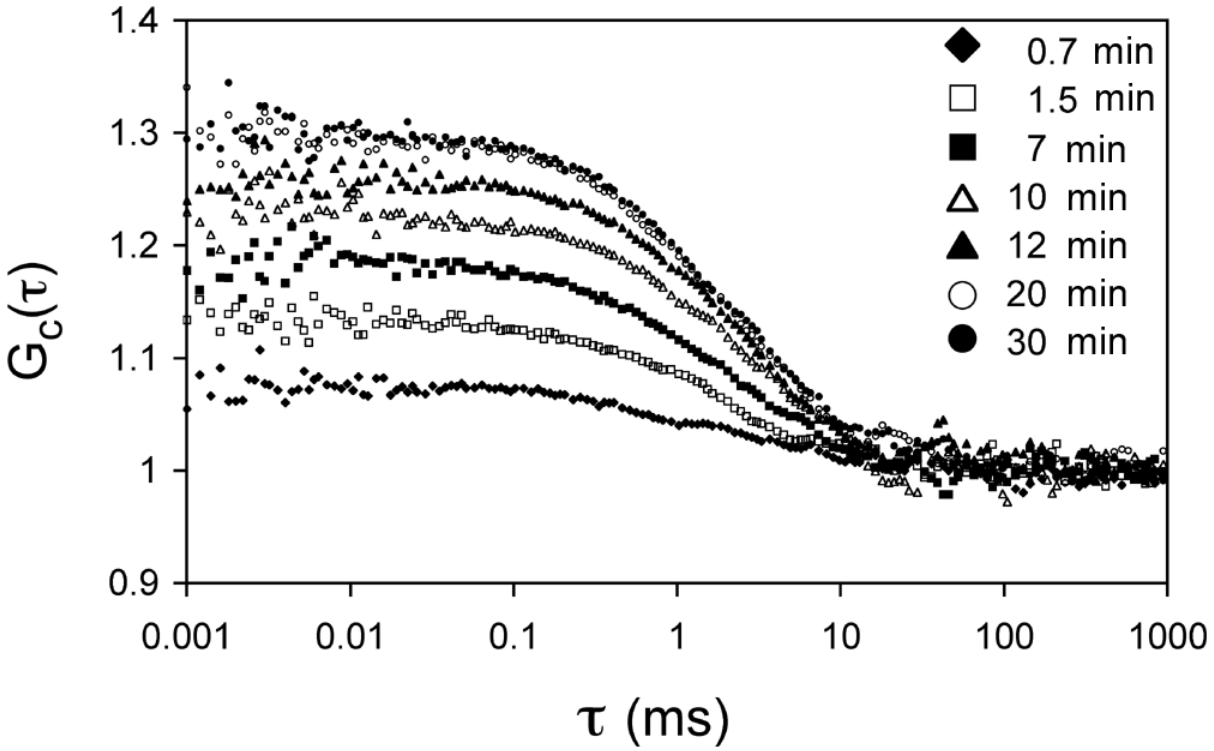
1.4
1.3
1.2
1.1
1
0.9
$G_c(\tau)$
0.001
0.01
0.1
1
10
100
1000
τ (ms)
0.7 min
1.5 min
7 min
10 min
12 min
20 min
30 min

Fig. 4

A

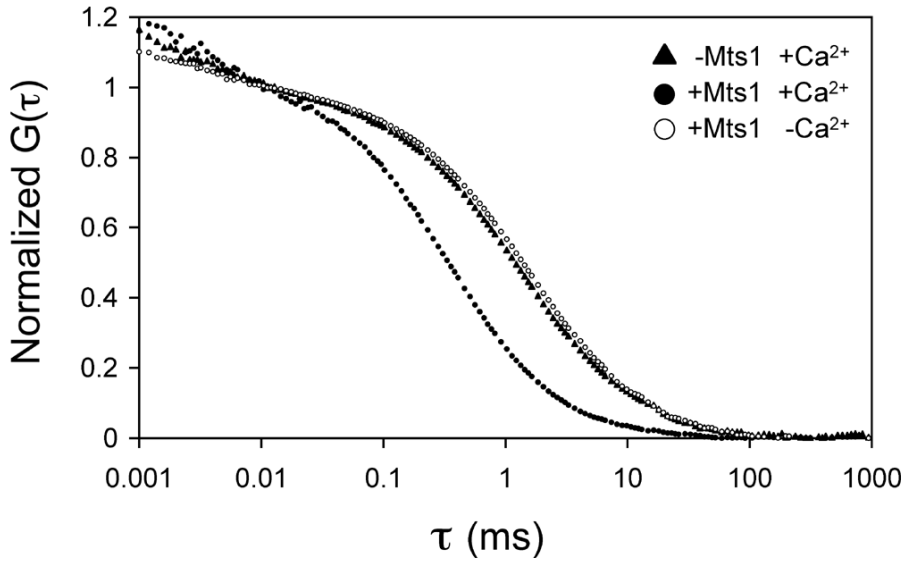
Normalized G(τ)
τ (ms)
-Mts1 +Ca2+
+Mts1 +Ca2+
+Mts1 -Ca2+
0
0.2
0.4
0.6
0.8
1
1.2
0.001
0.01
0.1
1
10
100
1000

B

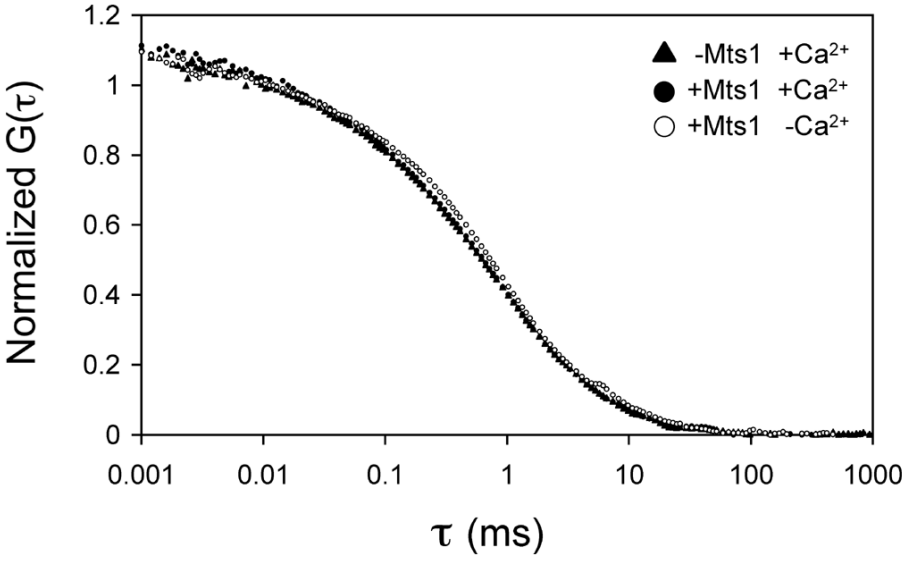
Normalized G(τ)
τ (ms)
-Mts1 +Ca2+
+Mts1 +Ca2+
+Mts1 -Ca2+
0
0.2
0.4
0.6
0.8
1
1.2
0.001
0.01
0.1
1
10
100
1000

Fig. 5

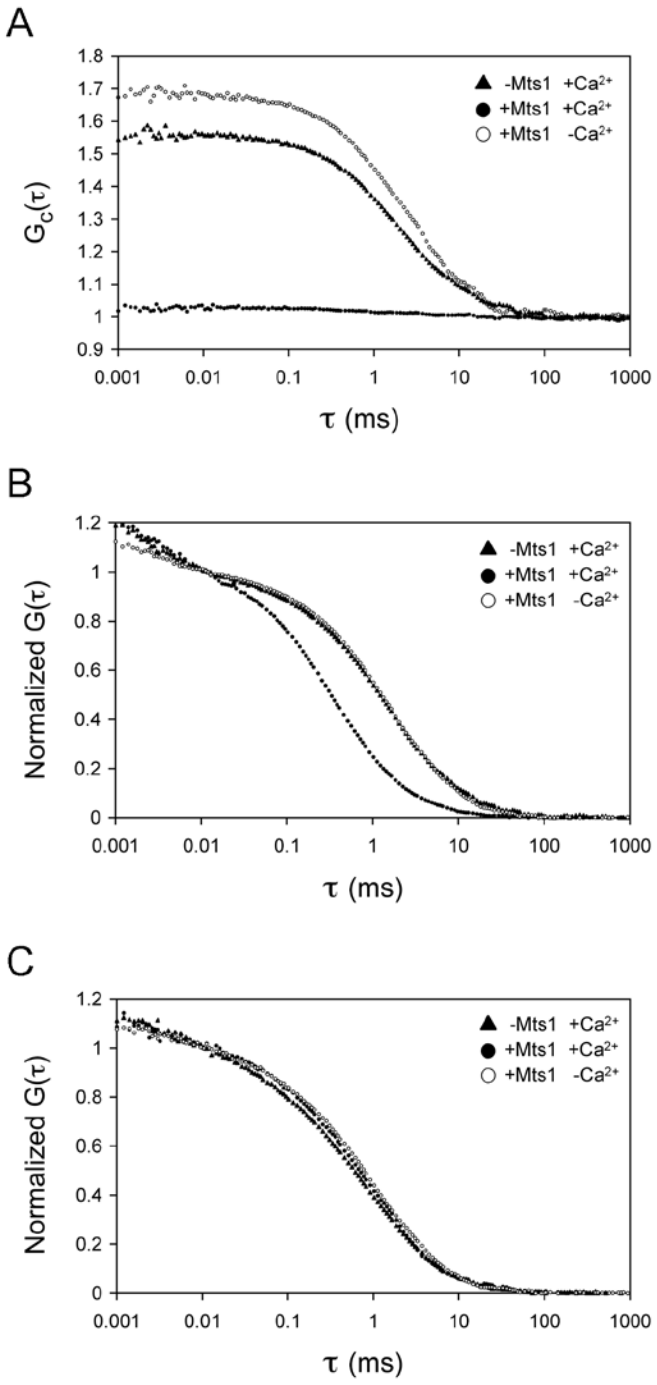
A
B
C
-Mts1 +Ca2+
+Mts1 +Ca2+
+Mts1 -Ca2+
Gc(τ)
Normalized G(τ)
τ (ms)
0.001
0.01
0.1
1
10
100
1000

Fig. 6